PAPER

Check for updates

Formation of monomeric Sn(ii) and Sn(iv) perfluoropinacolate complexes and their characterization by ^{119}Sn Mössbauer and ^{119}Sn NMR spectroscopies†

Jessica K. Elinburg,[a] Ariel S. Hyre,[a] James McNeely,[a] Todd M. Alam,[b] Steffen Klenner,[c] Rainer Pöttgen,[c] Arnold L. Rheingold[d] and Linda H. Doerrer [ID] *[a]

The synthesis and characterization of a series of Sn(ii) and Sn(iv) complexes supported by the highly electron-withdrawing dianionic perfluoropinacolate (pin^F) ligand are reported herein. Three analogs of $[Sn^{IV}(pin^F)_3]^{2-}$ with NEt$_3$H$^+$ (**1**), K$^+$ (**2**), and {K(18C6)}$^+$ (**3**) counter cations and two analogs of $[Sn^{II}(pin^F)_2]^{2-}$ with K$^+$ (**4**) and {K(15C5)$_2$}$^+$ (**5**) counter cations were prepared and characterized by standard analytical methods, single-crystal X-ray diffraction, and ^{119}Sn Mössbauer and NMR spectroscopies. The six-coordinate Sn^{IV}(pin^F) complexes display ^{119}Sn NMR resonances and [119]Sn Mössbauer spectra similar to SnO$_2$ (cassiterite). In contrast, the four-coordinate Sn^{II}(pin^F) complexes, featuring a stereochemically-active lone pair, possess low ^{119}Sn NMR chemical shifts and relatively high quadrupolar splitting. Furthermore, the Sn(ii) complexes are unreactive towards both Lewis bases (pyridine, NEt$_3$) and acids (BX$_3$, Et$_3$NH$^+$). Calculations confirm that the Sn(ii) lone pair is localized within the 5s orbital and reveal that the Sn 5p$_x$ LUMO is energetically inaccessible, which effectively abates reactivity.

Introduction

Tin has a wide variety of modern uses, keeping its complexes as an active area of research in both molecular and materials chemistry. Sn(iv) is more frequently employed in catalysis than Sn(ii),[1] although the important Mukaiyama aldol reaction was originally developed with Sn(ii) triflate as a mediator.[2–7] Forty years of development have since led to a diverse field of other catalysts for asymmetric synthesis,[8–10] but Sn(ii) species are still commonly used as reducing agents[1] and precursors for materials synthesis.[11–14] Sn(iv) and Sn(ii) molecular species are very important in investigations of precursors to SnO$_x$

anodes[15,16] and nanowires,[17] and to FTO (fluorine-doped tin oxide).[18] In such work, all O-donor coordination environments, {SnO$_n$}, for both Sn(ii) and Sn(iv) are highly sought after to minimize contamination of the resultant materials. Alkoxide ligands are often used in these efforts and numerous homo–[19,20] and heteroleptic[21–23] Sn alkoxide complexes have been prepared and older work reviewed.[24,25] Fluorinated alkoxides have also been investigated, almost exclusively monodentate ones, due to the increased volatility that fluorinated ligands afford their complexes.[26–28]

In recent years, our group has extensively utilized fluorinated O-donor monodentate ligands to stabilize a variety of transition metal centers.[29–39] These fluorinated alkoxides are highly electron-withdrawing and are weaker π-donors than their protio analogs, diminishing (μ-OR) bridging in complexes. They are electronically equivalent to fluoride (F$^-$) and lack C–H bonds susceptible to oxidative decomposition.[29] The structure and reactivity of 3d metal complexes of bidentate perfluoropinacolate, abbreviated (pin^F)$^{2-}$, have also been investigated.[31,35,37] In this work, we extend our studies into the p-block metallic elements and report the synthesis, characterization, and computational analysis of the monomeric Sn(iv) and Sn(ii) perfluoropinacolate complexes, $[Sn(pin^F)_3]^{2-}$ and $[Sn(pin^F)_2]^{2-}$. We also explore the unusual stability of $[Sn(pin^F)_2]^{2-}$ towards both Lewis acids and bases effected by the perfluoropinacolate ligand.

[a]Department of Chemistry, Boston University, 590 Commonwealth Avenue, Boston, MA 02215, USA. E-mail: doerrer@bu.edu
[b]Department of Organic Material Science, Sandia National Laboratories, Albuquerque, NM 87185, USA
[c]Institut für Anorganische und Analytische Chemie, Universität Münster, Corrensstrasse 30, D-48149 Münster, Germany
[d]Department of Chemistry and Biochemistry, University of California, San Diego, 9500 Gilman Drive, MC 0332, La Jolla, CA 92093, USA

Some homoleptic Sn complexes with O-donor bidentate ligands are known, including catecholate,[40,41] acetylacetonate,[42,43] and oxalate,[44,45] but whose characterization with regard to Sn has primarily focused on the geometries and connectivity. Organometallic Sn complexes have been studied by both ^{119}Sn NMR[46] and ^{119}Sn Mössbauer spectroscopy,[47] as have Sn amides, Sn(IV),[48] Sn(IV) peptides[49–51] and Sn(II),[48,52] but very rarely have both of these spectroscopic techniques been applied to coordination complexes such as Sn alkoxides. To the best of our knowledge, only two Sn(IV) alkoxide examples with this characterization exist,[53,54] as well as one Sn(II) example.[55] Therefore, this work contributes important characterization data to the growing family of $\{SnO_n\}$ compounds and potential SnO_x precursors.

Results and discussion

Synthesis of $[Sn(pin^F)_3]^{2-}$ and $[Sn(pin^F)_2]^{2-}$ complexes

Perfluoropinacolate complexes of Sn(IV) were synthesized according to the top of Scheme 1. Historically, the preparation of tin alkoxides has largely relied upon $SnCl_4$ as the tin source, though extensive investigation has found that often, the chloride ligands are not completely displaced, leading to the formation of heteroleptic complexes.[24] Nevertheless, the preparation of homoleptic tetra-alkoxides has been achieved via alcholysis, which is especially straightforward when the pK_a of the added alcohol is lower than that of the liberated alcohol.

Our synthesis entails the partial alcoholysis of $Sn(O^tBu)_4$ with H_2pin^F along with the addition of two equivalents of additional base to complete the deprotonation of the dianionic ligand. As the source of the counter cation, the base can be selected to tune the solubility and steric properties of the resultant complex. Herein, we report the synthesis and characterization of three Sn(IV) $[Sn(pin^F)_3]^{2-}$ complexes with different counter-cations: NEt_3H^+ (**1**), K^+ (**2**), $\{K(18\text{-crown-}6)\}^+$ (**3**), and due to the chelate effect, the preferential binding of the dianionic, bidentate $(pin^F)^{2-}$ ligand over $(O^tBu)^-$ was presumed. However, initial attempts to synthesize the Sn(IV) complexes at room temperature proved unsuccessful. These results led us to pursue solvothermal syntheses. Optimization of the reaction conditions found that heating the reaction mixtures to 100 °C for 8 h in toluene, followed by slow cooling of the reaction autoclaves precipitated near-quantitative yields of colorless
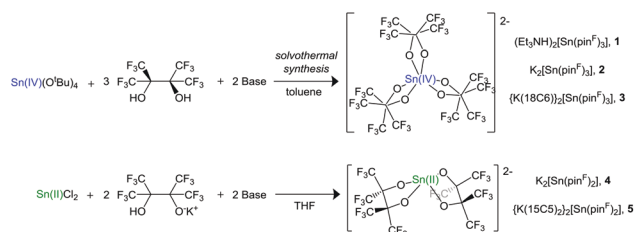
crystals directly from the reaction mixture. Subsequent recrystallization of these isolated crystals from acetone/hexanes led to the isolation of analytically pure, X-ray quality crystals.

Perfluoropinacolate complexes of Sn(II) were synthesized according to the bottom of Scheme 1. These reactions were carried out under inert atmosphere, and unlike the reactions with Sn(IV), proceed at room temperature. The order of addition in these reactions proved crucial. Initial addition of the ligand salt $KHpin^F$ to $SnCl_2$ led to the formation of a significantly volatile intermediate, presumed to be the Sn(II) complex of mono-deprotonated perfluoropinacol, $Sn(Hpin^F)_2$, and quantitative yields of byproduct salt, KCl. In order to form the desired $[Sn(pin^F)_2]^{2-}$ complex, full deprotonation of the ligand, followed by the addition of $SnCl_2$ is required. We have prepared both $K_2[Sn(pin^F)_2]$ and its fully-encapsulated analog, $\{K(15C5)_2\}_2[Sn(pin^F)_2]$. In both cases, crystallization of crude solids from THF/hexanes produces colorless crystals, although residual $SnCl_2$ proved challenging to separate. The $[Sn(pin^F)_2]^{2-}$ complexes are unsurprisingly highly air-sensitive, decomposing rapidly upon exposure to oxygen or moisture. In fact, exposing a concentrated solution of the Sn(II) complex to air for several hours leads to the precipitation of crystals of the analogous $[Sn(pin^F)_3]^{3-}$ complex in low yields, which we have confirmed via X-ray crystallography.

Structure of $[Sn(pin^F)_3]^{2-}$ and $[Sn(pin^F)_2]^{2-}$ complexes

Compounds **1–5** have all been characterized with single-crystal X-ray diffraction. Important bond lengths and angles are summarized in Table 1, and crystallographic data collection and refinement parameters are in Table S1.† The Sn(IV)-containing anion $[Sn(pin^F)_3]^{2-}$ (Fig. 1, left) has been crystallized as three distinct analogs differing by counter-cation: Et_3NH^+ (**1**), K^+ (**2**), and $K(18C6)^+$ (**3**). Compounds **1–3** represent the first example of a metal center coordinated to three sterically-bulky perfluoropinacolate ligands. Complexes **1–3** are distorted trigonal prisms with O_6 coordination around the Sn(IV) center. The average Sn–O bond distances are very similar for all of the Sn(IV) complexes: 2.06 Å, 2.04 Å, and 2.05 Å, for **1**, **2**, and **3**, respectively. Similarly, the maximum and minimum O–Sn–O bond angles are similar for all three compounds, with maximum O–Sn–O bond angles spanning a range of 2.8° and minimum O–Sn–O bond angles differing by only 0.6° between the compounds. While explicit structural parameterization exists for four- and five-coordinate compounds[56,57] (namely, τ_4 and τ_5, respectively), a related parameterization, known as the twist angle, is available for six-coordinate compounds.[58] Twist angle is defined as the displacement in alignment of the ligand groups, where 0° indicates a perfectly-aligned (trigonal prismatic) configuration and 60° indicates a completely staggered (octahedral) configuration. Calculation of the twist angle for the six-coordinate Sn(IV) complexes indicates that all complexes are distorted trigonal prisms, with the twist angles ranging from 31.2° to 34.0°, intermediate between an octahedron and trigonal prism.
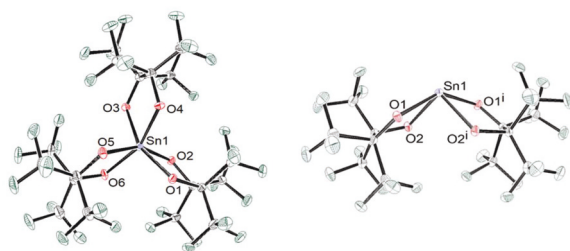
Each Sn(IV) analog crystallizes with a different number of acetone molecules coordinated to the counter-cations.

Scheme 1 Synthesis of Sn(II) and Sn(IV) perfluoropinacolate complexes.

Table 1 Selected bond distances (Å) and angles (°) for Sn(II) and Sn(IV) pin^F complexes

	1 [Et$_3$NH]$_2$[Sn(pin^F)$_3$]	**2** K$_2$[Sn(pin^F)$_3$]	**3** {K(18C6)}$_2$[Sn(pin^F)$_3$]	**4** K$_2$[Sn(pin^F)$_2$]	**5** {K(15C5)$_2$}$_2$[Sn(pin^F)$_2$]
Sn–O(1)	2.0620(15)	2.039(2)	2.070(2)	2.298(2)	2.2385(16)
Sn–O(2)	2.0516(15)	2.047(3)	2.042(3)	2.132(2)	2.1209(17)
Sn–O(3)	2.0536(15)	2.041(3)	2.045(3)		
Sn–O(4)	2.0525(16)		2.043(2)		
Sn–O(5)	2.0620(16)		2.068(3)		
Sn–O(6)	2.0487(16)		2.063(3)		
O–Sn–O (min-max)	78.37(10)–158.03(10)	78.97(6)–157.91(6)	78.43(10)–160.75(1)	72.99(8)–141.85(12)	74.02(6)–145.11(9)
Twist angle58	34.0	31.6	31.2		

Fig. 1 ORTEP of the [Sn(pin^F)$_3$]$^{2-}$ anion in **1** (left) and the [Sn(pin^F)$_2$]$^{2-}$ anion in **5** (right). Counter-cations and solvent molecules omitted for clarity. Ellipsoids are shown at the 50% probability level.

Compound **1** crystallizes with two acetone molecules; as shown in Fig. S1,† each is hydrogen-bonded to one NEt$_3$H$^+$ counter-cation through the interaction of an oxygen atom of acetone to the weakly acidic hydrogen atom of NEt$_3$H$^+$. Uniquely, **2** crystallizes with three acetone molecules in which the oxygen atoms of two solvent molecules coordinate to a single K$^+$ in a bridging fashion; the remaining acetone molecule coordinates the other K$^+$ counter-cation as shown in Fig. S2.† This configuration produces a quasi-oligomeric structure. Finally, **3** crystallizes with one acetone molecule coordinated to a single 18-crown-6-encapsulated K$^+$ counter-cation (Fig. S3†). As confirmed *via* elemental analysis, upon placing the complexes under vacuum, **1** and **2** retain their solvent coordination while **3** desolvates quickly, presumably due to the reduced Lewis acidity of the K$^+$ cation upon encapsulation by the crown ether.

Both K$_2$[Sn(pin^F)$_2$] (**4**) and its fully-encapsulated cation equivalent, {K(15C5)$_2$}$_2$[Sn(pin^F)$_2$] (**5**), have also been structurally characterized (Fig. 1, right). Both complexes exhibit {SnO$_4$} coordination around the Sn(II) center and adopt a distorted square pyramid geometry, owing to the presence of a stereochemically-active lone pair of electrons on the metal center. The average Sn–O bond distances are similar for both Sn(II) complexes: 2.22(8) Å (**4**) and 2.18(6) Å (**5**). Compared to the Sn(IV) complexes, the Sn–O bond distances are elongated by approximately 0.15 Å in the reduced species, which is expected due to the weakened ligand–metal electrostatic interactions in Sn(II) *vs.* Sn(IV). K⋯F interactions between the counter-cation and ligand are present in **4** but are not observed in **5**.

The range of maximum and minimum O–Sn–O bond angles in the Sn(II) compounds is more pronounced than that of Sn(IV). The maximum O–Sn–O angle of **5** is 3.26 Å larger than that of **4** and the minimum O–Sn–O angle of **5** is 1.03 Å larger than that of **4**. This observed expansion of the SnO$_4$ unit upon encapsulation of the counter-cation may be attributed to the absence of K⋯F interactions within the molecule.

The Sn(II) complexes also co-crystallize with solvent molecules as shown in Fig. S4 and S5.† Interestingly, in both cases, Lewis basic O-donor solvent molecules do not interact with the Sn(II) center. Instead, **4** crystallizes with two THF molecules, each coordinated to a single K$^+$ counter-cation. **5** co-crystallizes with two THF molecules suspended symmetrically below the O$_4$ plane.

The binding of two bidentate, dianionic ligands to the divalent tin center in [Sn(pin^F)$_2$]$^{2-}$ is structurally and electronically unique. Sn(II) complexes with multi-anionic ligands are not commonly seen in the literature; most are dimers, polymers, or clusters, and overall neutral,[22,59–61] although a Sn(II) complex featuring a single tetradentate corrole ligand was synthesized by Yun and coworkers in 2014.[62] Other coordination environments featuring multiple monoanionic ligands are more likely to promote the formation of charged species of divalent tin; examples include the three-coordinate complex [Sn(OC$_4$F$_9$)$_3$]$^-$, which has been reported and crystallized with several counterions,[26] and [SnCl$_3$]$^-$, which has been used in ionic liquids[63,64] and to stabilize five-coordinate platinum.[65,66] Thus, the characterization of [Sn(pin^F)$_2$]$^{2-}$ provides a unique opportunity to study the coordination environment and electronic structure of divalent tin imparted by the dianionic, bidentate perfluoropinacolate ligand.

^{119}Sn Mössbauer spectroscopy

In order to investigate the electronic structure of the complexes, ^{119}Sn Mössbauer spectra of complexes containing both the [Sn(pin^F)$_3$]$^{2-}$ and [Sn(pin^F)$_2$]$^{2-}$ anions were obtained (Fig. 2 and Fig. S6†); the corresponding fitting parameters are tabulated in Table 2. Tetravalent complexes **1–3** exhibit single signals with isomer shifts around 0.1 mm s^{-1}. The geometric environment of Sn in the SnO$_6$ core, which falls between octahedral and trigonal prismatic geometry, is comparable to cassiterite, SnO$_2$, which shows an isomer shift of 0 mm s^{-1}.[67] Similar values were summarized by Zuckerman for a variety of tetravalent organotin compounds.[68] The small distortions of the SnO$_6$ cores from an ideal octahedron (ideal cubic symmetry) are reflected in the small quadrupole splitting para-
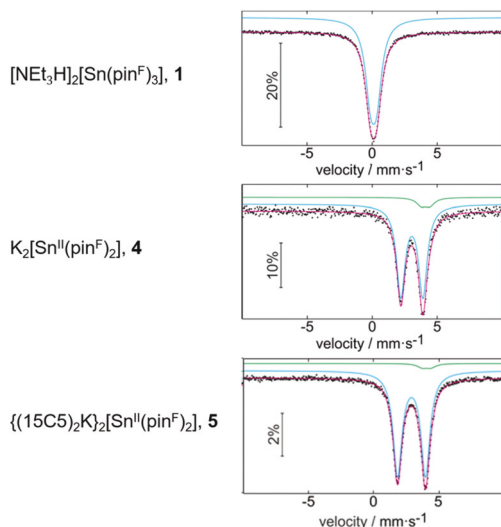
Paper

Fig. 2 ^{119}Sn Mössbauer spectra of (top to bottom) **1**, **4**, and **5**.

Fig. 3   Comparison of ^{119}Sn Mössbauer data from **4**, **5**, and literature compounds. References and detailed formulae in Table S2.†

Table 2 Fitting parameters of ^{119}Sn Mössbauer spectroscopic measurements at 6 K. δ = isomer shift, ΔE_Q = electric quadrupole splitting, Γ = experimental line width. Data marked with an asterisk were kept fixed during the fitting procedure

	δ/mm s^{-1}	ΔE_Q/mm s^{-1}	Γ/mm s^{-1}	Ratio/%
1 [NEt$_3$H]$_2$[Sn(pin^F)$_3$]	0.103(3)	0.44(1)	1.00(1)	100
2 K$_2$[Sn(pin^F)$_3$]	0.122(1)	0.356(5)	0.927(5)	100
3 {K(18C6)}$_2$[Sn(pin^F)$_3$]	0.106(1)	0.468(4)	0.975(6)	100
4 K$_2$[Sn^{II}(pin^F)$_2$]	3.044(3)	1.698(6)	0.792(9)	92(1)
SnCl$_2$	4.1*	0.66*	0.9*	8(1)
5 {(15C5)$_2$K}$_2$[Sn^{II}(pin^F)$_2$]	2.940(1)	2.153(2)	0.863(4)	96(1)
SnCl$_2$	4.1*	0.66*	0.9*	4(1)

meters. The experimental line width parameters fall in a similar range to previously reported data.[68]

The ^{119}Sn Mössbauer spectra of the divalent complexes **4** and **5** are shown in Fig. 2 and are quite different than the Sn (IV) complexes. The spectrum of **4** was well reproduced by a superposition of two sub-spectra in 92 : 8 ratio, indicating a small amount of residual SnCl$_2$ in the sample. The main signal corresponds to the Sn(II) atoms of K$_2$[Sn^{II}(pin^F)$_2$]. The lower tin valence leads to a substantial shift of the s electron density and the isomer shift increases to 3.044(3) mm s^{-1}. The lone-pair character present within the distorted SnO$_4$ square pyramids leads to substantial quadrupole splitting of 1.698(6) mm s^{-1}. The slightly quadrupole-split signal of the educt was included in the fit with fixed parameters taken from the original literature.[69,70] The data for the {K(15C5)$_2$}$_2$[Sn^{II}(pin^F)$_2$] sample is quite similar with a slightly lower isomer shift of 2.940(1) mm s^{-1}, and again contains a small amount of SnCl$_2$ carried along. The quadrupole splitting parameter of 2.153(2) mm s^{-1} indicates a slightly more asymmetric coordination of the tin site as compared to K$_2$[Sn^{II}(pin^F)$_2$].

Fig. 3 shows the range of ^{119}Sn Mössbauer isomer shifts and quadrupole splittings from a wide range of chemical compounds in the literature, largely Sn(II) species, as well as the
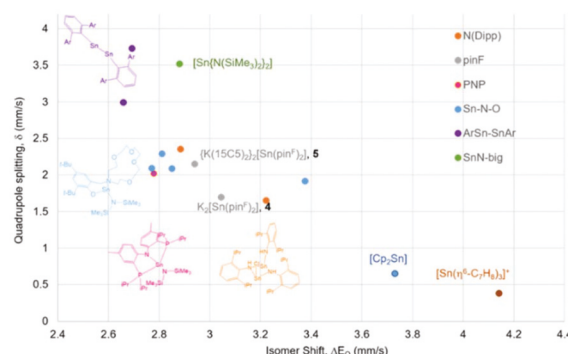
values for **4** and **5**. Details for all compounds, including Mössbauer spectroscopic parameters, compound structural formulae, CSD codes, and references are given in Table S2.† This plot shows that, as previously demonstrated,[47,71] most Sn (II) compounds have isomer shifts above ~2.5 mm s^{-1} and the quadrupole splittings can vary widely, depending on the chemical environment.[72] Compounds **4** and **5** have similar isomer shifts to each other, which are also similar to other literature compounds with moderately basic ligands, but do not resemble the organometallic compounds [Cp$_2$Sn], [Cp*$_2$Sn], or [Sn(η^6-C$_7$H$_8$)$_3$]$^+$ which have noticeably higher isomer shifts but significantly smaller quadrupole splittings. In the opposite corner of Fig. 3 are the useful starting material [Sn{N (SiMe$_3$)$_2$}$_2$] and two Sn–Sn bonded species, ArSn–SnAr, all of which have smaller isomer shifts and much larger quadrupole splittings.

^{119}Sn and ^{19}F NMR spectroscopy

Solution-state ^{119}Sn NMR. Solution-state ^{119}Sn NMR spectra of **1–5** in C$_4$D$_8$O (d_8-THF) were obtained; their chemical shifts are summarized in Table 3. The chemical shifts observed for the Sn(IV) alkoxides (**1–3**) range from approximately −480 ppm to −510 ppm. While these shifts are typical of tetravalent tin alkoxides, the difference in shifts among the three complexes was interesting, because they differ only by the counter-ion. To explore this phenomenon, the observed chemical shift was compared with both the twist angle and average Sn–O bond

Table 3 Solution-state ^{119}Sn NMR data for **1–5** at 298 K. In the case of **5**, the ^{119}Sn NMR spectrum displays an additional peak at −140 ppm. This feature appears to be Sn(II) associated with crown ether or an oligomeric species

Complex	^{119}Sn Chemical Shift (ppm) vs. Me$_4$Sn (δ = 0 ppm)
1 [NEt$_3$H]$_2$[Sn(pin^F)$_3$]	−503.6
2 K$_2$[Sn(pin^F)$_3$]	−511.2
3 {K(18C6)}$_2$[Sn(pin^F)$_3$]	−482.4
4 K$_2$[SnII(pin^F)$_2$]	−435.0
5 {(15C5)$_2$K}$_2$[SnII(pin^F)$_2$]	−500.9, (−140.0)

distance of each complex, but such comparison failed to reveal a clear trend.

Although the scope of complexes investigated by ^{119}Sn NMR is largely comprised of tetravalent tin species, there has been some investigation of Sn(II) complexes. The divalent tin halides have been well-studied, and their chemical shifts range from approximately 0 to 600 ppm. Comparatively, the chemical shifts observed for **4** (−435.0 ppm) and **5** (−500.9 ppm) fall nearly 1000 ppm up-field (lower frequency) from the classically-studied SnX$_2$, indicating a significantly more electron-shielded tin environment. More recently, several Sn(II) alkoxy- and amido-alkoxy-complexes of various coordination number and nuclearity have been characterized *via* ^{119}Sn NMR. When examining the chemical shifts of these compounds (largely compiled by Boyle *et al.*),[17] a clear trend emerges—an increase in coordination number around the tin center results in a markedly up-field shift in the NMR resonance, regardless of ligand identity.

Wang *et al.* have prepared three-coordinate Sn(II) alkoxy- and amido-alkoxy complexes, including the homoleptic dimer [Sn(μ-OSiPh$_3$)(OSiPh$_3$)]$_2$, which exhibits a ^{119}Sn NMR chemical shift of −338 ppm.[73] Boyle and coworkers have prepared two four-coordinate homoleptic Sn(II) alkoxides complexes, [Sn(μ-oMP)$_2$]$_\infty$ (oMP = 2-methylphenolate) and [Sn (μ-oPP)$_2$]$_\infty$ (oPP = 2-isopropylphenolate), with major chemical shifts of −412 ppm and −429.2 ppm, respectively.[17] It should be noted, however, that like many tin alkoxides, these complexes exist as bridged polymeric chains rather than monomeric complexes. Overall, the exceptionally low frequency ^{119}Sn NMR chemical shift observed for monomers **4** and **5** is likely resultant of the unique binding motif imparted by the dianionic (pin^F)$^{2-}$ ligand.

Variable-temperature (VT) ^{19}F NMR spectroscopy. The room temperature ^{19}F NMR spectra of complexes **1–5** contain multiple resonances, indicating the presence of several unique fluorine environments within the complexes. To further probe this observation, variable-temperature ^{19}F NMR studies were carried out (Fig. S7†). For **1–3**, three ^{19}F environments are present at low temperature (270 K). Upon heating to near room temperature, the two lowest-frequency resonances coalesce to produce a spectrum with two peaks. As the temperature is further increased (up to 340 K), these resonances ultimately coalesce at 296 K (**1**), 326 K (**2**), and 316 K (**3**). Although the exact origin of the multiple fluorine environments remains unclear, we postulate that this dynamic averaging most likely stems from a combination of ligand exchange between axial and equatorial positions, as well as averaging of rotational configurations of the CF$_3$ ligands. This exchange appears to be dependent on the counter-cation, with rates of exchange for **1** > **2** ≈**3**.

Similar to the Sn(IV) complexes, **5** exhibits fluxional behavior, although two ^{19}F NMR resonances persist even at high temperature; no ultimate coalescence is observed. Interestingly, **4** does not exhibit fluxional behavior. This is perhaps attributed to the presence of strong K···F interactions between the counter-cation and ligand, which restrict ligand movement.

Solid-state [119]Sn magic angle spinning (MAS) NMR spectroscopy. To further investigate the electronic anisotropy induced by the stereochemically-active lone pair of electrons residing at the Sn(II) center of **4** and **5**, solid-state [119]Sn magic angle spinning (MAS) NMR measurements were performed. The ^{119}Sn MAS NMR spectrum of **4** is shown in Fig. 4 (top). The isotropic value of −460.7 ppm is shifted from the solution-state chemical shift of −435.0 ppm, the chemical shift anisotropy (CSA) was −635 ppm, and the asymmetry parameter (η$_{CS}$) was found to be 0.01. The spectrum of **5** (Fig. 4, bottom) is more complex due to an impurity present in the sample; this same impurity was present in solution-state measurements and spectral deconvolution was successfully performed.
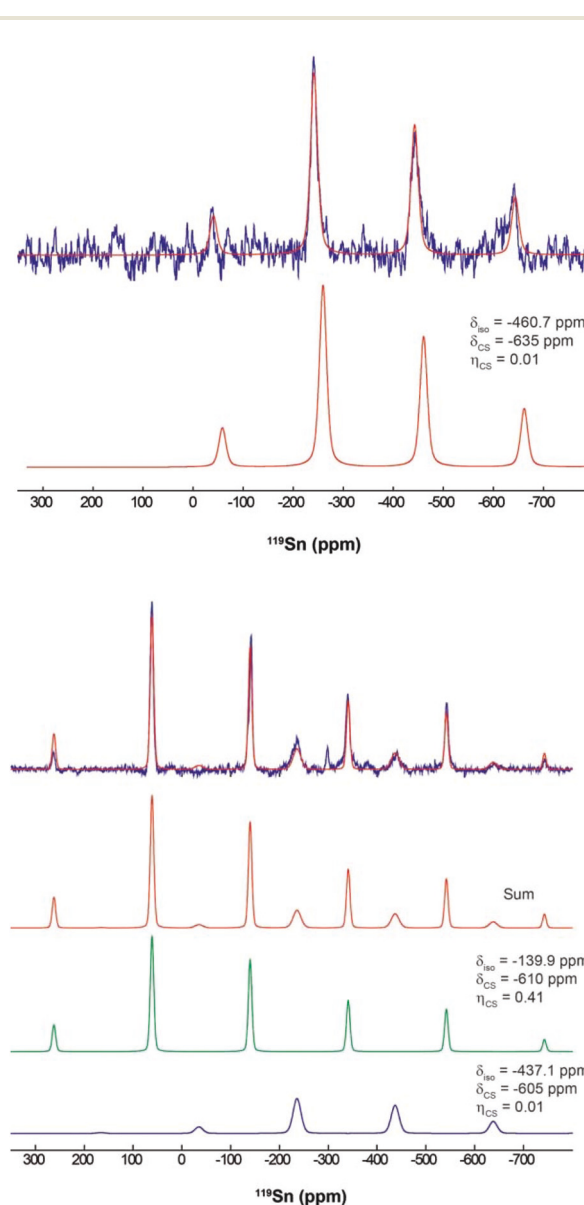

Fig. 4 Solid-state magic angle spinning (MAS) ^{119}Sn NMR spectra of **4** (top) and **5** (bottom) collected using 4 K scan averages with between 2 and 60 s recycle delays and referenced to external SnO$_2$ (δ = −603 ppm).

For **5** (represented by the blue trace), the isotropic value of −437.1 ppm is shifted from the solution-state chemical shift of −500.9 ppm. Similar to **4**, a significant CSA of −610 ppm with a low asymmetry of $\eta_{CS} = 0.01$ was observed.

Probing the Lewis acidity/basicity of $[\text{Sn}(\text{pin}^F)_2]^{2-}$

Canonically, coordination complexes of Sn(II) have been of interest due to the dichotomous presence of both a stereochemically active lone pair of electrons and an empty p orbital at the metal center. Among divalent tin compounds, $[\text{Sn}(\text{pin}^F)_2]^{2-}$ is among a very small number of monomeric O-donor complexes with a coordination number greater than three and there has been little investigation into their respective reactivities.

Donaldson and Grimes have suggested that the use of d orbitals to increase the coordination of Sn(II) above three is unlikely, due to the comparative energy gaps between the s, p, and d orbitals of tin; the s–d energy gap (−14 eV) is twice as large as the s–p energy gap (−7 eV).[74] For $[\text{Sn}(\text{pin}^F)_2]^{2-}$, this would imply that the unhybridized p orbital must be involved in ligand binding to facilitate the O_4 coordination of the Sn(II) center by the bidentate, dianionic $(\text{pin}^F)^{2-}$ ligand.

Even from our initial attempts to synthesize $[\text{Sn}(\text{pin}^F)_2]^{2-}$, we noted several intriguing observations about the behavior of the complex. Firstly, solutions of the complex seemed to adhere to Celite, making it nearly impossible to filter reactions using filter agent. Because Celite is comprised largely of weakly acidic silica and alumina particles, we began to postulate that our Sn(II) complex may behave as a Lewis base, rather than a Lewis acid. Furthermore, the crystal structures of **4** and **5** reveal that donor solvents, such as THF, co-crystallize with **4** and **5**, but do not interact with the Sn(II) center, further suggesting a lack of Lewis acidity. To probe this hypothesis, **4** was reacted with several Lewis acids and bases according to Scheme 2.

Interestingly, $[\text{Sn}(\text{pin}^F)_2]^{2-}$ did not create adducts with either Lewis acids (BBr_3, NEt_3H^+) or bases (pyridine, triethylamine). In fact, addition of NEt_3HCl simply resulted in a counter-ion exchange reaction, rather than forming a formally Sn(IV) terminal hydride complex, in which the original K^+ counter-ions were replaced by NEt_3H^+ and quantitative KCl salt precipitated from solution. Furthermore, addition of pyridine did not lead to a Sn(II) complex with pyridine bound at the metal center, but rather, pyridine associated with the K^+ counter ions. The unexpected stability of $[\text{Sn}(\text{pin}^F)_2]^{2-}$ in the presence of acids/bases suggests that the Sn(II) lone pair is localized in the 5s orbital, rendering it inert, and the Lewis acidity of the vacant p orbital is diminished. In order to further understand the stability afforded by the apparently unique electronic structure of $[\text{Sn}(\text{pin}^F)_2]^{2-}$, computational analysis was pursued.

Computational studies

As an initial prediction, the Sn(II) center of **4** was expected to have a lone pair in its 5s orbital and empty 5p orbitals. Natural Localized Molecular Orbital (NLMO, Fig. 5) analysis confirms that the lone pair orbital is highly localized (approximately 88%) tin 5s, with a further ~9% 5p character. NBO analysis further suggests that the interaction between the ligating oxygen atoms and the tin center are best described as polar covalent or dative, with the density much more localized on the oxygen atoms. Corroboration of this hypothesis is provided by bond order analysis, as all three methods (MBO, WBO, and NBI) found that each of the four Sn–O interactions have bond orders significantly lower than unity. Furthermore, the natural electron configuration of the tin center shows a population of 0.80 e in the 5p orbital, while the anionic O atoms of the ligands have 2p populations of approximately 5.16 e.

Canonical molecular orbital (MO) analysis of **4** shows that the lone pair of electrons on the Sn(II) center resides in the highest-occupied molecular orbital (HOMO), and confirms that it is primarily of tin 5s character, with approximately 15% contribution from the $5p_z$ atomic orbital (AO). The rest of the metal's 5p orbitals are distributed among the unoccupied MOs; the lowest-unoccupied molecular orbital (LUMO) is of primarily tin $5p_x$ character and is 4.35 eV higher in energy than the HOMO (Fig. 5 and 6). Although the lone pair is more
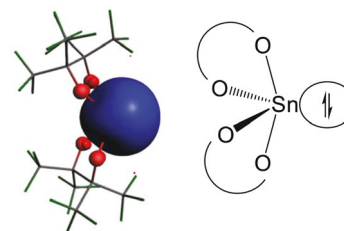

Fig. 5 NLMO visualization of the lone pair orbital of Sn(II) for **4** (left), with a diagram for clarity (right). Isosurface rendered at a value of 0.03.
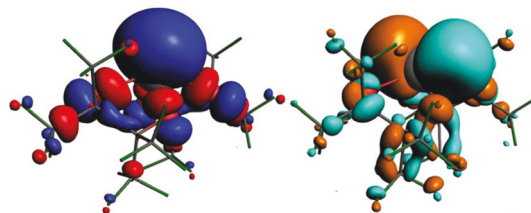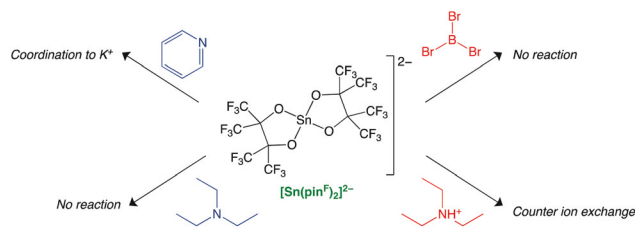

Fig. 6 Visualizations of the canonical HOMO (left) and LUMO (right) of **4**. Counter-cation and solvent molecules removed for clarity. Isosurfaces rendered at a value of 0.03.

Scheme 2 Reactions of $[\text{Sn}(\text{pin}^F)_2]^{2-}$ with Lewis acids and bases.

sterically available, it is expected to be relatively inert due to its high s character.

This lack of reactivity of $[Sn(pin^F)_2]^{2-}$ with Lewis acids was further explored by comparing its electronic structure and energies with the experimentally observed five-coordinate Sn(II) adduct with borane reported by Lappert *et al.*[75] We first note that Lappert's bare monomer has a significantly higher amount of 5p hybridization in the Sn(II) lone pair (NLMO, 21%). This would be expected to make the orbital more diffuse and capable of interacting with a Lewis acid. Furthermore, the MEPs for the two species (Fig. S8†) reveal a clear region in Lappert's species that is capable of interacting with a Lewis acid, but in $[Sn(pin^F)_2]^{2-}$ this is not the case. This enhanced hybridization and favorable electrostatic interactions observed in Lappert's compound help to rationalize why the largely unhybridized 5s orbital in $[Sn(pin^F)_2]^{2-}$ is so unreactive.

Computational analysis of four-coordinate Sn(II) complexes including Sn(saldph) (saldph = N,N'-(4,5-dimethyl-1,2-phenylene)bis(salicylideneiminato),[76] Sn(trop)$_2$ (trop = tropolone), and Sn(malt)$_2$ (malt = maltol)[77] reveals that while the Sn $5p_x$ orbital is empty in these systems as well, the energy of the $5p_x$ orbital in $[Sn(pin^F)_2]^{2-}$ is much higher than that observed for the other cases (Fig. S9†). This observation is likely due to the bidentate, dianionic pin^F ligand. Calculations reveal that F electron density from a nearby CF$_3$ group on the pin^F ligand is donated into the $5p_x$ orbital; this internal mesomeric effect (Fig. 7) effectively raises the energy of the $5p_x$ LUMO of $[Sn(pin^F)_2]^{2-}$, rendering it energetically inaccessible and unreactive toward Lewis bases. Similar calculations for the hypothetical $[Sn(pin^H)_2]^{2-}$ species show that this orbital is even higher in energy than the pin^F species, likely due to the lack of electron-withdrawing power of the ligands and the resultant stronger σ-bonding interactions with the p orbitals on Sn.

The ^{119}Sn Mössbauer spectroscopic data in Fig. 2 and Table 2 show highly unusual quadrupole splitting, ΔE_Q, for the two Sn(II)-containing compounds, **4** and **5**. Calculations of different structures and their attendant ^{119}Sn Mössbauer spectra were undertaken to understand what effect the counter-cations could have on the Sn(II) centers. As discussed above, the difference between the structures of **4** and **5** is the cation interactions and how the anion structure is perturbed by greater or lesser K$^+$ bonding with the pin^F O and F atoms. A
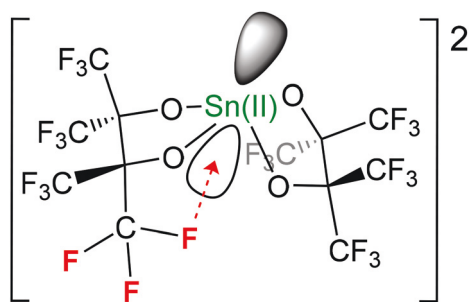
single O–Sn–O angle was chosen as the measure of distortion around the Sn(II) atom, namely the O$_2$–Sn–O$_4$ angle.

A potential energy surface (PES) for the uncoordinated dianion $[Sn(pin^F)_2]^{2-}$ is shown in Fig. 8. Two distinct energetic minima for the dianion exist, corresponding to O$_2$–Sn–O$_4$ bond angles of approximately 110° and 148°, respectively (red trace). The experimental structures of the two divalent Sn species **4** and **5** studied in this work lie in different minima. Compound **4** has an O$_2$–Sn–O$_4$ angle of 99.3°, closer to the higher-energy local minimum calculated for the dianion. On the other hand, **5** has an O$_2$–Sn–O$_4$ angle of 145.1°, a value close to the 148° minimum calculated for the dianion.

Furthermore, ΔE_Q as a function of the O$_2$–Sn–O$_4$ bond angle was calculated for the theoretical dianion (blue trace). These calculations predict that quadrupolar splitting for **4** and **5** should be approximately 1.9 and 1.5 mm s^{-1} respectively, based on their actual O$_2$–Sn–O$_4$ bond angles from their crystal structures. While the experimental quadrupolar splitting observed for **4** (1.698 mm s^{-1}) is lower than the dianion-based calculated value, the experimental value (2.153 mm s^{-1}) is much higher. We thus conclude that the Mössbauer spectroscopic parameters are far more sensitive to the geometry in this higher-energy region of the PES, with O–Sn–O angles less than 120°. Fig. 9 shows that after the counter-cations present in $\{K(15C5)_2\}_2[Sn^{II}(pin^F)_2]$ are introduced, the second, higher-energy minimum observed for $[Sn^{II}(pin^F)_2]^{2-}$ near 140° is removed, and the structure is limited to a single conformer that has a quadrupolar splitting highly sensitive to a O$_2$–Sn–O$_4$ angle less than 125°.

Given the sensitivity of the quadrupolar splitting to geometry, particularly at the lower O$_2$–Sn–O$_4$ angles, a number of different theories and basis sets were tested (see ESI†) for the prediction of Mössbauer spectroscopic parameters on the experimental structures of **4** and **5**. The best agreement was found with *ab initio* models. We have calculated the quadrupolar splitting as 1.639/1.746 mm s^{-1} and 1.785/1.853 mm s^{-1}
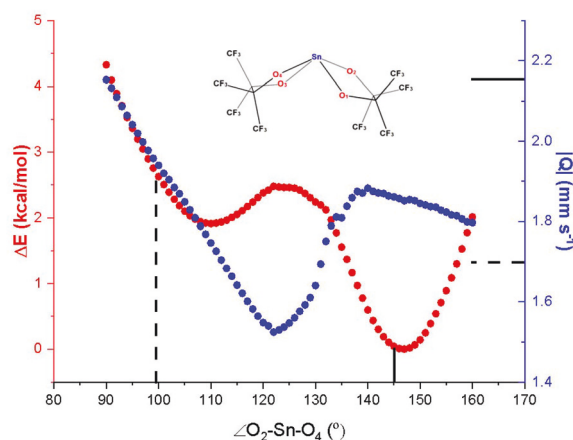

Fig. 7 Electron donation from F on the pin^F ligand into the p_x orbital on Sn(II) in **4** and **5**.

Fig. 8 PES for uncoordinated $[Sn^{II}(pin^F)_2]^{2-}$ (red dots) with corresponding quadrupolar splitting (blue dots). Dashed black lines highlight the corresponding angle/quadrupolar splitting for **4** and solid black lines highlight the angle/quadrupolar splitting for **5**.
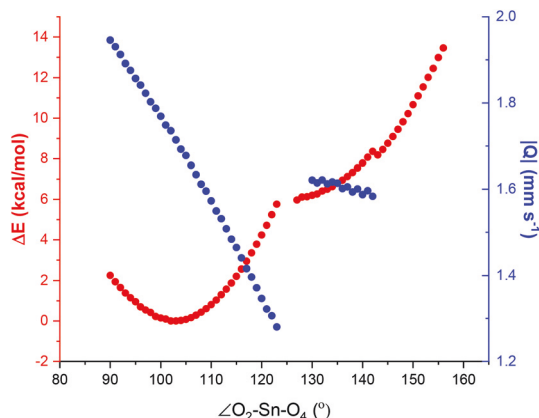
Fig. 9 PES for **4** (red dots) with corresponding quadrupolar splitting (blue dots).

for **4** and **5** respectively at the MP2/DLPNO-CCSD[78–82] levels with relaxed/unrelaxed densities. Because the experimental trend was reproduced, we can conclude that the experimentally observed discrepancy between **4** and **5** is most likely due to a local effect and not due to the extended structure of the system. This is supported by the failure of model that embedded the dianions in a 3 × 3 × 3 sea of CHELPG point charges to improve upon the results.

A comparison of the calculated ^{119}Sn Mössbauer quadrupole splitting *versus* the Sn electronic structure is informative. Fig. 10 illustrates how the electronic structure changes as the O–Sn–O angle changes. As mentioned above, the Sn(II) center has its lone-pair in an orbital predominantly 5s in character. The change in hybridization of this orbital is measured by the increase in 5p character. This hybridization reaches a minimum (highest amount of 5s character) when the O_2–Sn–O_4 bond angle is approximately 120°. The largest O–Sn–O angle of 145°, in **5**, also corresponds to the largest ΔE_Q, and therefore the greatest degree of hybridization at Sn. In **4**, the angle is smaller, the hybridization is less, and the ΔE_Q is also

smaller. We attribute this enhanced hybridization to a structural feature that differentiates the two conformers. For the less stable minimum (110°), the closest Sn–F contact is 3.14 Å, while this distance increases to 3.24 Å at the global minimum (147°). These increased Sn–F distances are also observed when comparing the two experimental structures. As the Sn–F distance lengthens, one would expect the energy of the $5p_y$ orbital to decrease, and thus increase its ability to hybridize the *s* orbital. This change is evidenced by the energy of the $5p_y$ orbital at the 110° and 147° geometries, which decreases from 6.138 eV to 5.993 eV when moving from 110° to 147°.

Experimental

General procedures

All Sn(IV) complexes were prepared in air; their solvothermal syntheses were carried out in Teflon-lined steel autoclaves in a Watlow 982 Cascade Tek programmable oven. Synthesis and manipulations of Sn(II) complexes were performed in an N_2-filled MBraun glove box. For the Sn(IV) complexes, solvents toluene, acetone, and hexanes were dried over 3 Å molecular sieves and used without further purification. For Sn(II) complexes, anhydrous solvents THF and hexanes were dried in an alumina-based solvent purification system (SPS) under Ar, piped directly into the N_2-filled dry box, and stored over 3 Å molecular sieves. Toluene was dried by refluxing over Na/benzophenone under N_2, distilling, and storing over 3 Å molecular sieves. $SnCl_2$ was dried by stirring in acetic anhydride, filtering, washing with dry Et_2O, and drying under vacuum. 15-Crown-5 was stored over 3 Å molecular sieves under N_2. H_2pin^F was purchased from Oakwood Chemicals and stored over 3 Å molecular sieves. The ligand salt, $KHpin^F$ was synthesized and recrystallized according to an established procedure.[36] NMR samples were prepared under N_2 using CD_3CN and C_4D_8O stored over 3 Å molecular sieves under N_2. All other reagents were obtained commercially and used with further purification. Elemental analyses were performed by Atlantic Microlabs, Inc. in Norcross, GA.

^{119}Sn Mössbauer spectroscopy

^{119}Sn Mössbauer spectroscopic investigations utilized a $Ca^{119m}SnO_3$ source with an activity of 5 mCi. The samples were placed in PMMA containers, the thickness of which was optimized according to Long *et al.*[83] A palladium foil of 0.05 mm thickness was used to reduce the tin K X-rays concurrently emitted by this source. The measurement was performed in a continuous flow cryostat system (Janis Research Co, LLC) at 6 K. The source was kept at room temperature. Fitting of the spectra was performed with the Win Normos for Igor6 software package.[84] The counting time was 1 day for each ^{119}Sn spectrum.

^{1}H, ^{19}F, and ^{119}Sn NMR spectroscopy

^{1}H NMR studies were carried out using a Varian 500 MHz NMR instrument at 298 K. Chemical shifts were referenced to
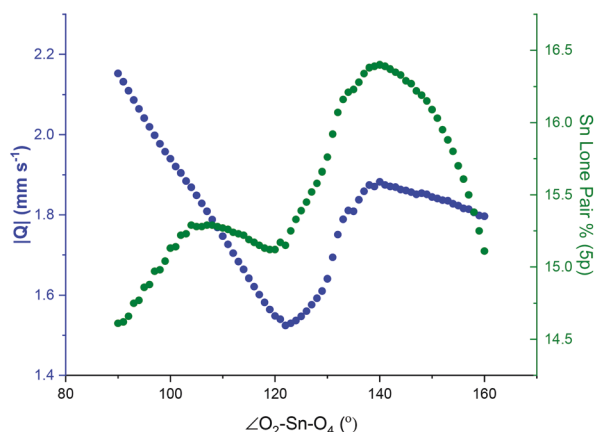

Fig. 10 Correlation between the Mössbauer quadrupolar splitting and the hybridization of the Sn(II) lone pair orbital for the PES displayed in Fig. 8.

the resonance of the residual solvent protons. Solution ^{119}Sn and ^{19}F NMR studies were carried out using a Bruker Avance III 600 MHz NMR instrument operating at 223.686 and 564.647 MHz for ^{119}Sn and ^{19}F, respectively. All measurements were carried out at 298 K, except for variable temperature ^{19}F measurements, which were collected at temperatures ranging from 260 to 340 K. A 5 mm broadband probe with the high frequency channel tuned to ^{19}F was utilized with no ^{1}H decoupling employed. The direct 1D ^{119}Sn NMR spectra were obtained using single pulse Bloch decay, ^{19}F GARP (Globally Optimized Alternating Phase Rectangular Pulse) decoupling, 10 μs π/2 pulse, 10 s recycle delay, with between 128 and 512 scan averages. The ^{19}F NMR spectra were obtained using 20 s recycle delay with 8 scan averages. The ^{119}Sn chemical shifts were referenced to external standard SnMe$_4$ (δ = 0.0 ppm) and the ^{19}F chemical shifts were referenced to the external standard CFCl$_3$ (δ = 0.0 ppm).

Solid-state ^{119}Sn magic angle spinning (MAS) measurements were carried out on a Bruker Avance III 400 MHz NMR instrument using a 2.5 mm triple resonance MAS probe spinning at 30 kHz with high power ^{19}F TPPM (two-pulse phase-modulated) decoupling. Spectra were obtained with 4 K scan averages with between 2 and 60 s recycle delays, depending on the relaxation time of each compound. The solid-state ^{19}F MAS NMR spectra were obtained on a Bruker Avance III 400 MHz NMR instrument using a 2.5 triple resonance MAS probe spinning at 20 kHz, with high power ^{1}H TPPM decoupling. The ^{19}F MAS NMR spectra were obtained using 16 K scan averages with 2 s recycle delays. The ^{119}Sn MAS NMR chemical shifts were referenced to the secondary external reference SnO$_2$ (δ = −603 ppm)[85] with respect to SnMe$_4$ (δ = 0.0 ppm) and the ^{19}F chemical shifts were referenced to the secondary external standard ammonium trifluoroacetate (δ = −72.0 ppm) with respect to CFCl$_3$ (δ = 0.0 ppm).

Computational studies

Gas-phase geometry optimizations were performed at the B3LYP level of theory with Gaussian16, Revision A.03.[86] The 6-311++G basis set was used for H, C, O, F, and K atoms, and Sn was treated with a Def2-TZVPPD/ECP-28 basis.[87] Starting coordinates for all complexes were obtained from their crystal structures. Natural Bond Orbital (NBO) analysis was carried out on gas-phase optimized structures with the NBO 6.0 package[88] and Bader analysis[89,90] as implemented in the 2016 release of the Amsterdam Density Functional (ADF) program suite.[91,92] The PBE level of theory was used, and no solvent effects were applied. Sn atoms were treated with the all-electron QZ4P basis set and scalar zeroth-order regular approximation (ZORA) relativistic corrections as implemented by ADF.[93] The SZ basis set was used for H, and DZ for all other elements.[94] All canonical molecular orbital analysis was performed on ADF output from these single-point calculations as well. Potential energy surfaces (PES) for [Sn^{II}(pin^F)$_2$]$^{2-}$ and {K(THF)$_2$}[Sn^{II}(pin^F)$_2$] were generated at the TPSSh[95,96]/DEF2-TZVP(Sn)/DEF2-SVP(H,C,O,F,[K])[97,98]/D3BJ[99,100]/RIJCOSX[101,102] level with the ORCA quantum chemistry package.[103–105] The

quadrupolar splitting along the PES was then evaluated at the TPSS0[106]/cc-pwCVTZ-DK(Sn)[107]/cc-pVTZ-DK(H,C,O,F)[108]/[DKH-DEF2-TZVP(K)]/DKH2[109] level. All other computational details can be found in the ESI.†

Syntheses

[Et$_3$NH]$_2$[Sn(pin^F)$_3$]·2(CH$_3$)$_2$CO. In a Teflon-lined steel autoclave, Sn(O^{t}Bu)$_4$ (0.200 g, 0.486 mmol), Et$_3$N (0.098 g, 0.973 mmol) and H$_2$pin^F (0.488 g, 1.460 mmol) were suspended in 5 mL of toluene. The autoclave was then sealed and heated to 100 °C for 8 h. Slow cooling of the reaction autoclave from 100 to 20 °C over the course of 8 h, followed by further cooling to 5 °C for 12 h, led to the precipitation of colorless crystals from the reaction mixture. Recrystallization of the initial crystals by layering acetone/hexanes at 5 °C for 3 days yielded large, X-ray quality colorless needles (0.480 g, 69% yield). Anal. calcd for C$_{36}$H$_{44}$F$_{36}$N$_2$O$_8$Sn: C, 30.12; H, 3.09; N, 1.95. Found: C, 30.15; H, 2.98; N, 1.98. ^{1}H NMR (CD$_3$CN, 500 MHz), 1.26 ppm (t), 2.11 ppm (s), 3.15 ppm (q), 6.75 ppm (t); ^{19}F NMR (600 MHz, C$_4$D$_8$O), −69.7 ppm (t, broad), −70.6 ppm (s); ^{119}Sn NMR (600 MHz, C$_4$D$_8$O), −511.2 ppm (s).

K$_2$[Sn(pin^F)$_3$]·3(CH$_3$)$_2$CO. In a Teflon-lined steel autoclave, Sn(O^{t}Bu)$_4$ (0.200 g, 0.486 mmol), KO^{t}Bu (0.109 g, 0.973 mmol) and H$_2$pin^F (0.488 g, 1.460 mmol) were suspended in 5 mL of toluene. The autoclave was then sealed and heated to 100 °C for 8 h. Slow cooling of the reaction autoclave from 100 to 20 °C over the course of 8 h, followed by further cooling to 5 °C for 12 h, led to the precipitation of colorless crystals from the reaction mixture. Recrystallization of the initial crystals by layering acetone/hexanes at 5 °C for 3 days yielded large, X-ray quality colorless blocks (0.295 g, 49% yield). Anal. calcd for C$_{27}$H$_{18}$F$_{36}$K$_2$O$_9$Sn: C, 23.72; H, 1.33; N, 0.00. Found: C, 23.73; H, 1.16; N, 0.00. ^{1}H NMR (CD$_3$CN, 500 MHz), 2.16 ppm (s); ^{19}F NMR (600 MHz, C$_4$D$_8$O), −68.8 (s), −70.4 (s, broad); ^{119}Sn NMR (600 MHz, C$_4$D$_8$O) −482.4 ppm (s).

{K(18C6)}$_2$[Sn(pin^F)$_3$]·(CH$_3$)$_2$CO. In a Teflon-lined steel autoclave, Sn(O^{t}Bu)$_4$ (0.200 g, 0.486 mmol), KO^{t}Bu (0.109 g, 0.973 mmol), 18-crown-6 (0.231 g, 0.875 mmol) and H$_2$pin^F (0.488 g, 1.460 mmol) were suspended in 5 mL of toluene. The autoclave was then sealed and heated to 100 °C for 8 h. Slow cooling of the reaction autoclave from 100 to 20 °C over the course of 8 h, followed by further cooling to 5 °C for 12 h, led to the precipitation of colorless crystals from the reaction mixture. Recrystallization of the initial crystals by layering acetone/hexanes at 5 °C for 3 days yielded large, X-ray quality colorless blocks (0.415 g, 58% yield). Anal. calcd for C$_{42}$H$_{48}$F$_{36}$K$_2$O$_{18}$Sn: C, 29.30; H, 2.81; N, 0.00. Found: C, 29.10; H, 2.70; N, 0.00. ^{1}H NMR (CD$_3$CN, 500 MHz), 3.59 ppm (s); ^{19}F NMR (600 MHz, C$_4$D$_8$O), −68.5 (s), −70.3 (t, broad); ^{119}Sn NMR (600 MHz, C$_4$D$_8$O) −503.6 ppm (s).

K$_2$[Sn(pin^F)$_2$]·2C$_4$H$_8$O. In a N$_2$-filled drybox, KHpin^F (0.250 g, 0.672 mmol) and KO^{t}Bu (0.075 g, 0.672 mmol) were combined in 4 mL of THF, yielding a translucent, colorless solution. After stirring for 30 min, SnCl$_2$ (0.064 g, 0.336 mmol) dissolved in minimal THF was added to the solution dropwise. Immediately, the solution became hazy and pale yellow. After

stirring for 6 h, the solution was dried under vacuum and triturated twice with toluene. The resulting pale solid was redissolved in minimal THF and filtered to remove KCl. The resulting pale yellow filtrate was layered with hexanes and stored at −28 °C for 5 days, yielding colorless X-ray quality plates (0.138 g, 41% yield). Anal. calcd for $C_{12}F_{24}K_2O_4Sn$: C, 16.74; H, 0.00; N, 0.00. Found: C, 16.84; H, 0.00; N, 0.10. ^{19}F NMR (600 MHz, C_4D_8O), −70.5 ppm (s), −71.5 ppm (s); ^{119}Sn NMR (600 MHz, C_4D_8O), −435.0 ppm (s).

{K(15C5)}₂[Sn(pinᶠ)₂]·2C₄H₈O. In a N_2-filled drybox, KHpinᶠ (0.250 g, 0.672 mmol) and KOᵗBu (0.075 g, 0.672 mmol) were combined in 4 mL of THF, yielding a translucent, colorless solution. After stirring for 30 min, 15-crown-5 (0.296 g, 1.344 mmol) was added directly to the solution and the solution stirred for 1 h. $SnCl_2$ (0.064 g, 0.336 mmol) dissolved in minimal THF was added to the solution dropwise. Immediately, the solution became cloudy white. After stirring for 6 h, the solution was dried under vacuum and triturated twice with toluene. The resulting pale solid was redissolved in minimal THF and filtered to remove KCl. The resulting pale off-white filtrate was layered with hexanes and stored at −28 °C for 2 days, yielding colorless X-ray quality needles (0.206 g, 33% yield). Anal. calcd for $C_{52}H_{80}F_{24}K_2O_{24}Sn$: C, 35.85; H, 4.63; N, 0.00. Found: C, 35.39; H, 4.67; N, 0.00. ^{19}F NMR (600 MHz, C_4D_8O), −72.2 ppm (s), −74.4 ppm (t), −78.9 ppm (s); ^{119}Sn NMR (600 MHz, C_4D_8O), −500.9 ppm (s) and −140.0 ppm (s) (small impurity).

Conclusions

Our efforts in the synthesis, characterization, and reactivity of metal complexes stabilized by highly fluorinated O-donor ligands has largely focused on Earth abundant, first-row metals such as Fe, Co, Ni, Cu, and Zn. Recently, we have expanded our scope to include complexes of a p-block metal, Sn with the perfluoropinacolate ligand (pinᶠ), creating monomeric tris-pinᶠ Sn(IV) and bis-pinᶠ Sn(II) complexes. The Sn(IV) anion, $[Sn(pin^F)_3]^{2−}$ has been crystallized and characterized with K^+, $K(18C6)^+$, and NEt_3H^+ counter cations; ^{119}Sn NMR and Mössbauer spectroscopic measurements reveal that these electronic environments are similar to that in SnO_2 (cassiterite). Variable-temperature ^{19}F NMR confirms fluxional behavior of the F atoms on the pinᶠ ligand and the rates of exchange are dependent on the presence of K⋯F interactions present in each analog.

Two versions of the Sn(II) anion $[Sn(pin^F)_2]^{2−}$ have been prepared, with both K^+ and $\{K(15C5)_2\}^+$ counter cations. The complexes containing $[Sn(pin^F)_2]^{2−}$ display ^{119}Sn NMR resonances shifted exceptionally upfield compared to other divalent Sn alkoxides, as well as unusually large quadrupolar splitting in their respective ^{119}Sn Mössbauer spectra, afforded by the highly electron-withdrawing dianionic pinᶠ ligands. The Mössbauer spectra are more sensitive than ^{119}Sn NMR such that future studies may gain more from those data if crystallographic characterization is not possible. MAS ^{119}Sn NMR

spectra of the Sn(II) complexes corroborate the electronic anisotropy imparted by the stereochemically-active lone pair on Sn. $[Sn(pin^F)_2]^{2−}$ is surprisingly stable towards both Lewis acids and bases; calculations reveal that the lone pair is localized in the 5s orbital and that the LUMO of the system is the high-energy Sn(II) p_x orbital.

The five new Sn(II)/Sn(IV) complexes described herein possess relatively rare $\{Sn(II)O_4\}$ and $\{Sn(IV)O_6\}$ coordination environments by the highly electron-withdrawing, dianionic perfluoropinacolate ligand. Our hypothesis was two-fold, that (i) the fluorinated alkoxide ligands would generate complex types not known with perhydropinacolate and (ii) the resulting complexes would have distinct electronic structures and/or reactivities. Both aspects have proven true.

In particular, (1) the $\{Sn(II)O_4\}$ environment is unlike most other Sn(II) complexes in the literature, (2) both Sn(II) and Sn(IV) species have been thoroughly characterized by ^{119}Sn NMR (solution and solid state) and ^{119}Sn Mössbauer spectroscopies, (3) included is a rare direct comparative analysis of the electronic structure of both Sn(II) and Sn(IV) analogs stabilized by the same ligand, and (4) complexes with both oxidation states have been investigated with state-of-the-art computational analysis to offer explanation for the unusual character of the Sn(II) species.

Conflicts of interest

There are no conflicts to declare.

Acknowledgements

Notes and references

1 I. Shiina and H. Fukui, in *Acid Catalysis in Modern Organic Synthesis*, ed. H. Yamamoto and K. Ishihara, Wiley-VCH, 2008, vol. 1, ch. 10, pp. 517–550.

2 T. Mukaiyama, H. Uchiro and S. Kobayashi, *Chem. Lett.*, 1989, **18**, 1001–1004.

3 S. Kobayashi, Y. Fujishita and T. Mukaiyama, *Chem. Lett.*, 1989, **18**, 2069–2072.

4 T. Mukaiyama, H. Uchiro and S. Kobayashi, *Chem. Lett.*, 1989, **18**, 1757–1760.

5 S. Kobayashi, T. Sano and T. Mukaiyama, *Chem. Lett.*, 1989, **18**, 1319–1322.

6 S. Kobayashi and T. Mukaiyama, *Chem. Lett.*, 1989, **18**, 297–300.

7 I. Shiina, *Chem. Rec.*, 2014, **14**, 144–183.

8 S. Adachi and T. Harada, *Org. Lett.*, 2008, **10**, 4999–5001.

9 D. J. Averill and M. J. Allen, *Catal. Sci. Technol.*, 2014, **4**, 4129–4137.

10 T. Ollevier and B. Plancq, *Chem. Commun.*, 2012, **48**, 2289–2291.

11 I. Y. Ahmet, M. S. Hill, P. R. Raithby and A. L. Johnson, *Dalton Trans.*, 2018, **47**, 5031–5048.

12 R. Félix, N. Llobera-Vila, C. Hartmann, C. Klimm, M. Hartig, R. G. Wilks and M. Bär, *RSC Adv.*, 2018, **8**, 67–73.

13 D. Mudusu, K. R. Nandanapalli, S. R. Dugasani, J. W. Kang, S. H. Park and C. W. Tu, *RSC Adv.*, 2017, **7**, 41452–41459.

14 H. Wang, J. Wang, S. Xie, W. Liu and C. Niu, *Nanoscale*, 2018, **10**, 6159–6167.

15 P. Kitschke, A.-M. Preda, A. A. Auer, S. Scholz, T. Rüffer, H. Lang and M. Mehring, *Dalton Trans.*, 2019, **48**, 220–230.

16 S. Suh and D. M. Hoffman, *Inorg. Chem.*, 1996, **35**, 6164–6169.

17 T. J. Boyle, T. Q. Doan, L. A. M. Steele, C. Apblett, S. M. Hoppe, K. Hawthorne, R. M. Kalinich and W. M. Sigmund, *Dalton Trans.*, 2012, **41**, 9349–9364.

18 A. Verchère, S. Mishra, E. Jeanneau, H. Guillon, J.-M. Decams and S. Daniele, *Inorg. Chem.*, 2020, **59**, 7167–7180.

19 T. Fjeldberg, P. B. Hitchcock, M. F. Lappert, S. J. Smith and A. J. Thorne, *J. Chem. Soc., Chem. Commun.*, 1985, 939–941, DOI: 10.1039/C39850000939.

20 M. J. Hampden-Smith, T. A. Wark, A. Rheingold and J. C. Huffman, *Can. J. Chem.*, 1991, **69**, 121–129.

21 T. Zöller, L. Iovkova-Berends, C. Dietz, T. Berends and K. Jurkschat, *Chem. – Eur. J.*, 2011, **17**, 2361–2364.

22 T. J. Boyle, J. M. Segall, T. M. Alam, M. A. Rodriguez and J. M. Santana, *J. Am. Chem. Soc.*, 2002, **124**, 6904–6913.

23 T. J. Boyle, T. M. Alam, M. A. Rodriguez and C. A. Zechmann, *Inorg. Chem.*, 2002, **41**, 2574–2582.

24 M. J. Hampden-Smith, T. A. Wark and C. J. Brinker, *Coord. Chem. Rev.*, 1992, **112**, 81–116.

25 K. C. Molloy, *J. Chem. Res.*, 2008, 549–554, DOI: 10.3184/030823408X356846.

26 M. Schleep, C. Hettich, J. M. Glatz, D. Kratzert, W. Beichel, J. Velázquez Rojas, H. Scherer and I. Krossing, *Z. Anorg. Allg. Chem.*, 2019, **645**, 301–308.

27 A. Jana, H. W. Roesky, C. Schulzke and P. P. Samuel, *Organometallics*, 2010, **29**, 4837–4841.

28 M. Allan, A. F. Janzen and C. J. Willis, *Can. J. Chem.*, 1968, **46**, 3671–3677.

29 S. A. Cantalupo, J. S. Lum, M. C. Buzzeo, C. Moore, A. G. Di Pasquale, A. L. Rheingold and L. H. Doerrer, *Dalton Trans.*, 2010, **39**, 374–383.

30 S. A. Cantalupo, H. E. Ferreira, E. Bataineh, A. J. King, M. V. Petersen, T. Wojtasiewicz, A. G. DiPasquale, A. L. Rheingold and L. H. Doerrer, *Inorg. Chem.*, 2011, **50**, 6584–6596.

31 S. A. Cantalupo, S. R. Fiedler, M. P. Shores, A. L. Rheingold and L. H. Doerrer, *Angew. Chem., Int. Ed.*, 2012, **51**, 1000–1005.

32 J. S. Lum, P. E. Chen, A. L. Rheingold and L. H. Doerrer, *Polyhedron*, 2013, **58**, 218–228.

33 M. V. Petersen, A. H. Iqbal, L. N. Zakharov, A. L. Rheingold and L. H. Doerrer, *Polyhedron*, 2013, **52**, 276–283.

34 S. F. Hannigan, J. S. Lum, J. W. Bacon, C. Moore, J. A. Golen, A. L. Rheingold and L. H. Doerrer, *Organometallics*, 2013, **32**, 3429–3436.

35 L. Tahsini, S. E. Specht, J. S. Lum, J. J. M. Nelson, A. F. Long, J. A. Golen, A. L. Rheingold and L. H. Doerrer, *Inorg. Chem.*, 2013, **52**, 14050–14063.

36 S. F. Hannigan, A. I. Arnoff, S. E. Neville, J. S. Lum, J. A. Golen, A. L. Rheingold, N. Orth, I. Ivanovic-Burmazovic, P. Liebhaeuser, T. Roesener, J. Stanek, A. Hoffmann, S. Herres-Pawlis and L. H. Doerrer, *Chem. – Eur. J.*, 2017, **23**, 8212–8224.

37 J. L. Steele, L. Tahsini, C. Sun, J. K. Elinburg, C. M. Kotyk, J. McNeely, S. A. Stoian, A. Dragulescu-Andrasi, A. Ozarowski, M. Ozerov, J. Krzystek, J. Telser, J. W. Bacon, J. A. Golen, A. L. Rheingold and L. H. Doerrer, *Chem. Commun.*, 2018, **54**, 12045–12048.

38 S. E. N. Brazeau and L. H. Doerrer, *Dalton Trans.*, 2019, **48**, 4759–4768.

39 S. E. N. Brazeau, E. E. Norwine, S. F. Hannigan, N. Orth, I. Ivanovic-Burmazovic, D. Rukser, F. Biebl, B. Grimm-Lebsanft, G. Praedel, M. Teubner, M. Rubhausen, P. Liebhauser, T. Rosener, J. Stanek, A. Hoffmann, S. Herres-Pawlis and L. H. Doerrer, *Dalton Trans.*, 2019, **48**, 6899–6909.

40 R. R. Holmes, S. Shafieezad, V. Chandrasekhar, A. C. Sau, J. M. Holmes and R. O. Day, *J. Am. Chem. Soc.*, 1988, **110**, 1168–1174.

41 X. Sun, D. W. Johnson, D. L. Caulder, R. E. Powers, K. N. Raymond and E. H. Wong, *Angew. Chem., Int. Ed.*, 1999, **38**, 1303–1307.

42 V. G. Sevastyanov, E. P. Simonenko, P. A. Ignatov, V. S. Popov, A. V. Churakov, N. T. Kuznetsov and V. S. Sergienko, *Mendeleev Commun.*, 2012, **22**, 239–241.

43 M. C. Barry, C. M. Lieberman, Z. Wei, R. Clérac, A. S. Filatov and E. V. Dikarev, *Inorg. Chem.*, 2018, **57**, 2308–2313.

44 P. Ramaswamy, A. Datta and S. Natarajan, *Eur. J. Inorg. Chem.*, 2008, **2008**, 1376–1385.

45 S. Ayyappan, A. K. Cheetham and S. Natarajan, *Chem. Mater.*, 1998, **10**, 3746–3755.

46 R. Hani and R. A. Geanangel, *Coord. Chem. Rev.*, 1982, **44**, 229–246.

47 R. V. Parish, *Prog. Inorg. Chem.*, 1972, **15**, 101–200.

48 J. Henning, H. Schubert, K. Eichele, F. Winter, R. Poettgen, H. A. Mayer and L. Wesemann, *Inorg. Chem.*, 2012, **51**, 5787–5794.

49 P. Surdy, P. Rubini, N. Buzas, B. Henry, L. Pellerito and T. Gajda, *Inorg. Chem.*, 1999, **38**, 346–352.

50 F. Huber, M. Vornefeld, G. Ruisi and R. Barbieri, *Appl. Organomet. Chem.*, 1993, **7**, 243–252.

51 N. Buzas, L. Nagy, H. Jankovics, R. Kramer, E. Kuzmann, A. Vertes and K. Burger, *J. Radioanal. Nucl. Chem.*, 1999, **241**, 313–322.

52 W. A. Merrill, J. Steiner, A. Betzer, I. Nowik, R. Herber and P. P. Power, *Dalton Trans.*, 2008, 5905–5910, DOI: 10.1039/b809671f.

53 N. Bertazzi, G. Casella, P. D'Agati, T. Fiore, C. Mansueto, V. Mansueto, C. Pellerito, L. Pellerito and M. Scopelliti, *Appl. Organomet. Chem.*, 2008, **22**, 389–396.

54 A. G. Davies, L. Smith and P. J. Smith, *J. Organomet. Chem.*, 1972, **39**, 279–288.

55 V. Poirier, T. Roisnel, S. Sinbandhit, M. Bochmann, J.-F. Carpentier and Y. Sarazin, *Chem. – Eur. J.*, 2012, **18**, 2998–3013.

56 A. W. Addison, T. N. Rao, J. Reedijk, J. van Rijn and G. C. Verschoor, *Dalton Trans.*, 1984, 1349–1356, DOI: 10.1039/DT9840001349.

57 L. Yang, D. R. Powell and R. P. Houser, *Dalton Trans.*, 2007, 955–964, DOI: 10.1039/B617136B.

58 S. A. Kubow, K. J. Takeuchi, J. J. Grzybowski, A. J. Jircitano and V. L. Goedken, *Inorg. Chim. Acta*, 1996, **241**, 21–30.

59 L. Iovkova-Berends, T. Berends, C. Dietz, G. Bradtmöller, D. Schollmeyer and K. Jurkschat, *Eur. J. Inorg. Chem.*, 2011, **2011**, 3632–3643.

60 L. Iovkova-Berends, T. Berends, T. Zöller, G. Bradtmöller, S. Herres-Pawlis and K. Jurkschat, *Eur. J. Inorg. Chem.*, 2012, **2012**, 3191–3199.

61 S. Karwasara, C. K. Jha, S. Sinhababu and S. Nagendran, *Dalton Trans.*, 2016, **45**, 7200–7204.

62 L. Yun, H. Vazquez-Lima, H. Fang, Z. Yao, G. Geisberger, C. Dietl, A. Ghosh, P. J. Brothers and X. Fu, *Inorg. Chem.*, 2014, **53**, 7047–7054.

63 G. W. Parshall, *J. Am. Chem. Soc.*, 1972, **94**, 8716–8719.

64 M. Currie, J. Estager, P. Licence, S. Men, P. Nockemann, K. R. Seddon, M. Swadźba-Kwaśny and C. Terrade, *Inorg. Chem.*, 2013, **52**, 1710–1721.

65 R. V. Lindsey, G. W. Parshall and U. G. Stolberg, *J. Am. Chem. Soc.*, 1965, **87**, 658–659.

66 K. A. O. Starzewski and P. S. Pregosin, in *Catalytic Aspects of Metal Phosphine Complexes*, American Chemical Society, 1982, vol. 196, ch. 2, pp. 23–41.

67 P. E. Lippens, *Phys. Rev. B: Condens. Matter Mater. Phys.*, 1999, **60**, 4576–4586.

68 J. J. Zuckerman, Applications of 119mSn Mössbauer Spectroscopy to the Study of Organotin Compounds, in *Adv. Organomet. Chem*, 1971, vol. 9, pp. 21–134.

69 J. G. Ballard and T. Birchall, *Can. J. Chem.*, 1975, **53**(22), 3371–3373.

70 J. D. Donaldson, D. G. Nicholson and B. J. Senior, *J. Chem. Soc. A*, 1968, 2928–2931, DOI: 10.1039/J19680002928.

71 J. J. Zuckerman, in *Organotin-119m Moessbauer spectroscopy: the first quarter century*, Plenum, 1984, pp. 267–293.

72 E. A. V. Ebsworth, D. W. H. Rankin and S. Cradock, *Structural Methods in Molecular Inorganic Chemistry*, Blackwell Scientific Publications, 2nd edn, 1991.

73 L. Wang, C. E. Kefalidis, T. Roisnel, S. Sinbandhit, L. Maron, J.-F. Carpentier and Y. Sarazin, *Organometallics*, 2015, **34**, 2139–2150.

74 J. D. Donaldson and S. M. Grimes, in *Chemistry of Tin*, 1998, pp. 62–94, DOI: 10.1007/978-94-011-4938-9_3.

75 C. Drost, P. B. Hitchcock and M. F. Lappert, *Organometallics*, 1998, **17**, 3838–3840.

76 A. M. Vandenbergen, J. D. Cashion, G. D. Fallon and B. O. West, *Aust. J. Chem.*, 1990, **43**, 1559–1571.

77 M. C. Barret, M. F. Mahon, K. C. Molloy, J. W. Steed and P. Wright, *Inorg. Chem.*, 2001, **40**, 4384–4388.

78 F. Neese, A. Hansen and D. G. Liakos, *J. Chem. Phys.*, 2009, **131**, 064103.

79 L. M. J. Huntington, A. Hansen, F. Neese and M. Nooijen, *J. Chem. Phys.*, 2012, **136**, 064101.

80 F. Neese, F. Wennmohs and A. Hansen, *J. Chem. Phys.*, 2009, **130**, 114108.

81 C. Riplinger and F. Neese, *J. Chem. Phys.*, 2013, **138**, 034106.

82 C. Riplinger, B. Sandhoefer, A. Hansen and F. Neese, *J. Chem. Phys.*, 2013, **139**, 134101.

83 G. J. Long, T. Cranshaw and G. Longworth, *Mössbauer Effect Ref. Data J.*, 1983, **6**, 42–49.

84 R. A. Brand, WinNormos for Igor6 (version for Igor 6.2 or above: 22.02.2017), Universität Duisburg, 2017.

85 C. Cossement, J. Darville, J.-M. Gilles, J. B. Nagy, C. Fernandez and J.-P. Amoureux, *Magn. Reson. Chem.*, 1992, **30**, 263–270.

86 M. J. Frisch, G. W. Trucks, H. B. Schlegel, G. E. Scuseria, M. A. Robb, J. R. Cheeseman, G. Scalmani, V. Barone, G. A. Petersson, H. Nakatsuji, X. Li, M. Caricato, A. V. Marenich, J. Bloino, B. G. Janesko, R. Gomperts, B. Mennucci, H. P. Hratchian, J. V. Ortiz, A. F. Izmaylov, J. L. Sonnenberg, D. Williams-Young, F. Ding, F. Lipparini, F. Egidi, J. Goings, B. Peng, A. Petrone, T. Henderson, D. Ranasinghe, V. G. Zakrzewski, J. Gao, N. Rega, G. Zheng, W. Liang, M. Hada, M. Ehara, K. Toyota, R. Fukuda, J. Hasegawa, M. Ishida, T. Nakajima, Y. Honda, O. Kitao, H. Nakai, T. Vreven, K. Throssell, J. A. Montgomery Jr., J. E. Peralta, F. Ogliaro, M. J. Bearpark, J. J. Heyd, E. N. Brothers, K. N. Kudin, V. N. Staroverov, T. A. Keith, R. Kobayashi, J. Normand, K. Raghavachari, A. P. Rendell, J. C. Burant, S. S. Iyengar, J. Tomasi, M. Cossi, J. M. Millam, M. Klene, C. Adamo,

R. Cammi, J. W. Ochterski, R. L. Martin, K. Morokuma, O. Farkas, J. B. Foresman and D. J. Fox, *Gaussian 16, Revision A.03*, Wallingford, CT, 2016.

87 P. Simidzija, M. J. Lecours, R. A. Marta, V. Steinmetz, T. B. McMahon, E. Fillion and W. S. Hopkins, *Inorg. Chem.*, 2016, **55**, 9579–9585.

88 E. D. Glendening, J. K. Badenhoop, A. E. Reed, J. E. Carpenter, J. A. Bohmann, C. M. Morales, C. R. Landis and F. Weinhold, *NBO 6.0*, Theoretical Chemistry Institute, University of Wisconsin, Madison, 2013.

89 J. I. Rodríguez, R. F. W. Bader, P. W. Ayers, C. Michel, A. W. Götz and C. Bo, *Chem. Phys. Lett.*, 2009, **472**, 149–152.

90 J. I. Rodríguez, *J. Comput. Chem.*, 2013, **34**, 681–686.

91 C. Fonseca Guerra, G. J. Snijders, G. te Velde and J. E. Baerends, *Theor. Chem. Acc.*, 1998, **99**, 391–403.

92 G. te Velde, F. M. Bickelhaupt, E. J. Baerends, C. Fonseca Guerra, S. J. A. van Gisbergen, J. G. Snijders and T. Ziegler, *J. Comput. Chem.*, 2001, **22**, 931–967.

93 E. van Lenthe, A. Ehlers and E.-J. Baerends, *J. Chem. Phys.*, 1999, **110**, 8943–8953.

94 E. van Lenthe and E.-J. Baerends, *J. Comput. Chem.*, 2003, **24**, 1142–1156.

95 J. Tao, J. P. Perdew, V. N. Staroverov and G. E. Scuseria, *Phys. Rev. Lett.*, 2003, **91**, 146401.

96 V. N. Staroverov, G. E. Scuseria, J. Tao and J. P. Perdew, *J. Chem. Phys.*, 2003, **119**, 12129–12137.

97 F. Weigend and R. Ahlrichs, *Phys. Chem. Chem. Phys.*, 2005, **7**, 3297–3305.

98 F. Weigend, *Phys. Chem. Chem. Phys.*, 2006, **8**, 1057–1065.

99 S. Grimme, J. Antony, S. Ehrlich and H. Krieg, *J. Chem. Phys.*, 2010, **132**, 154104.

100 S. Grimme, S. Ehrlich and L. Goerigk, *J. Comput. Chem.*, 2011, **32**, 1456–1465.

101 F. Neese, F. Wennmohs, A. Hansen and U. Becker, *Chem. Phys.*, 2009, **356**, 98–109.

102 S. Kossmann and F. Neese, *Chem. Phys. Lett.*, 2009, **481**, 240–243.

103 F. Neese, *Wiley Interdiscip. Rev.: Comput. Mol. Sci.*, 2012, **2**, 73–78.

104 F. Neese, ORCA – An Ab Initio, DFT and Semiempirical SCF-MO Package, Version 4.0, Max Planck Institute for Chemical Energy Conversion, Mülheim a. d., Ruhr, Germany, 2017.

105 F. Neese, *Wiley Interdiscip. Rev.: Comput. Mol. Sci.*, 2018, **8**, e1327.

106 S. Grimme, *J. Phys. Chem.*, 2005, **109**, 3067–3077.

107 D. H. Bross and K. A. Peterson, *Theor. Chem. Acc.*, 2013, **133**, 1434.

108 W. A. d. Jong, R. J. Harrison and D. A. Dixon, *J. Chem. Phys.*, 2001, **114**, 48–53.

109 T. Nakajima and K. Hirao, *Chem. Rev.*, 2012, **112**, 385–402.